energy&fuels

pubs.acs.org/EF Article

Study on the Pore Structure and Fractal Dimension of Tight Sandstone in Coal Measures

Jingyi Wang, Fujie Jiang,* Chunlin Zhang, Zezhang Song,* and Wuling Mo

Cite This: *Energy Fuels* 2021, 35, 3887−3898 Read Online

ACCESS | Metrics & More | Article Recommendations

ABSTRACT: The pore structure directly controls the tight reservoir's physical properties and plays a crucial role in gas charging and accumulation. To characterize the pore structure accurately, it is critical for the exploration and development of tight gas. In this paper, the pore structure of a tight sandstone reservoir in the Carboniferous Benxi Formation coal-bearing strata in the Ordos Basin was characterized by X-ray diffraction, thin sections, scanning electron microscopy, high-pressure mercury intrusion, and X-ray−computed tomography techniques. The porosity and permeability of the Benxi Formation reservoir are 0.12−12.53% and 0.0003−33.59 mD, respectively. The type of pores is dominated by secondary pores, followed by primary pores and microcracks. The reservoirs are divided into three types based on the high-pressure mercury injection curve pattern and the displacement pressure. The average pore radii of Type I and Type II reservoirs are similar, and the pore volume, average radius of throats, and pore−throat connectivity ratio of Type II reservoirs are all higher than those of Type I from the results displayed by micron CT. The pores of the reservoir are divided into small pores (<1 μm), mesopores (0.1−1 μm), and macropores (>1 μm) according to their diameters. In type I reservoirs, three types of pores are found, and the type II reservoirs have mainly mesopores and macropores. There are almost no large pores in Type III reservoirs. Type I has the best porosity and the smallest heterogeneity, while Type II has stronger heterogeneity than Type I, according to the findings when combining the high-pressure mercury intrusion experiment with fractal theory. Total fractal dimension has a weak negative correlation with porosity and a positive correlation with permeability. The contribution rate of mesopores and macropores to porosity is more affected by heterogeneity. The seepage of a reservoir is mainly affected by the throat radius and throat connectivity ratio under the same porosity condition. With a larger throat radius and a higher throat connection ratio, the seepage capacity will be stronger. As the content of clay minerals increases, the heterogeneity of the reservoir increases and permeability decreases.

1. INTRODUCTION

With the increasing global demand for energy, the shortage of conventional oil and gas resources has become increasingly apparent. In the 1980s, more and more policies encouraged the development of unconventional oil and gas resources to supplement the energy gap.[1] The exploration and development process of unconventional oil and gas resources has been accelerated globally.[2−4] In 2016, the global unconventional natural gas resources (nearly 4000 × 10^{32} m^3) were 8 times the conventional ones (approximately 471 × 10^{12} m^3).[1,5,6] Tight sandstone is one of the world's primary strategic energy forms,[7] and its resources amount to 210 × 10^{12} m^3.[1,6] In China, 96% of the proven geological reserves of tight sandstone gas are in the Ordos and Sichuan basins,[5,8] of which more than one-third are related to coal-measure reservoirs. Tight sand in coal-measure gas is an unconventional natural gas in which coal bed or coal-measure shale is the source rock, and tight sandstone reservoirs are closely connected with coal-measure source rocks.[9] Coal-measure source rocks produce high acid, and the mass fraction of organic acids (11−95 mg/g) produced by them is significantly higher than that of mudstone (30−60 mg/g). The abundance of organic acid supply and the more intensive dissolution, which smooths the edges of the framework particles (quartz), results in the increased porosity.[9−11] Besides, III kerogen mainly produces gaseous hydrocarbons, and there is no problem of blocking pore throats and hindering the migration of gaseous hydrocarbons.[12] Strong rock cyclicity is one of the salient features of coal-measure strata. Repeating and alternating the lithofacies can form multiple sets of "source-reservoir-cap", which facilitate the generation, preservation, and enrichment of hydrocarbon gas and increase the compaction rate compared to that of lenticular sand bodies.[9−12] This strong diagenetic compaction changes the structure of the primary pores and reduces the average pore throat diameter, resulting in an increase in pore throat curvature and the number of isolated or disconnected pores, making the types of microscopic pores in the rock more complex.

Finding out the microstructure parameters that affect the reservoir and seepage capacity can help classify and evaluate the tight sandstone reservoirs reasonably, because hydrocarbon reserves, productivity, and final production yield are closely

Received: November 25, 2020
Revised: February 3, 2021
Published: February 17, 2021

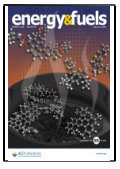

https://dx.doi.org/10.1021/acs.energyfuels.0c03991
Energy Fuels 2021, 35, 3887−3898

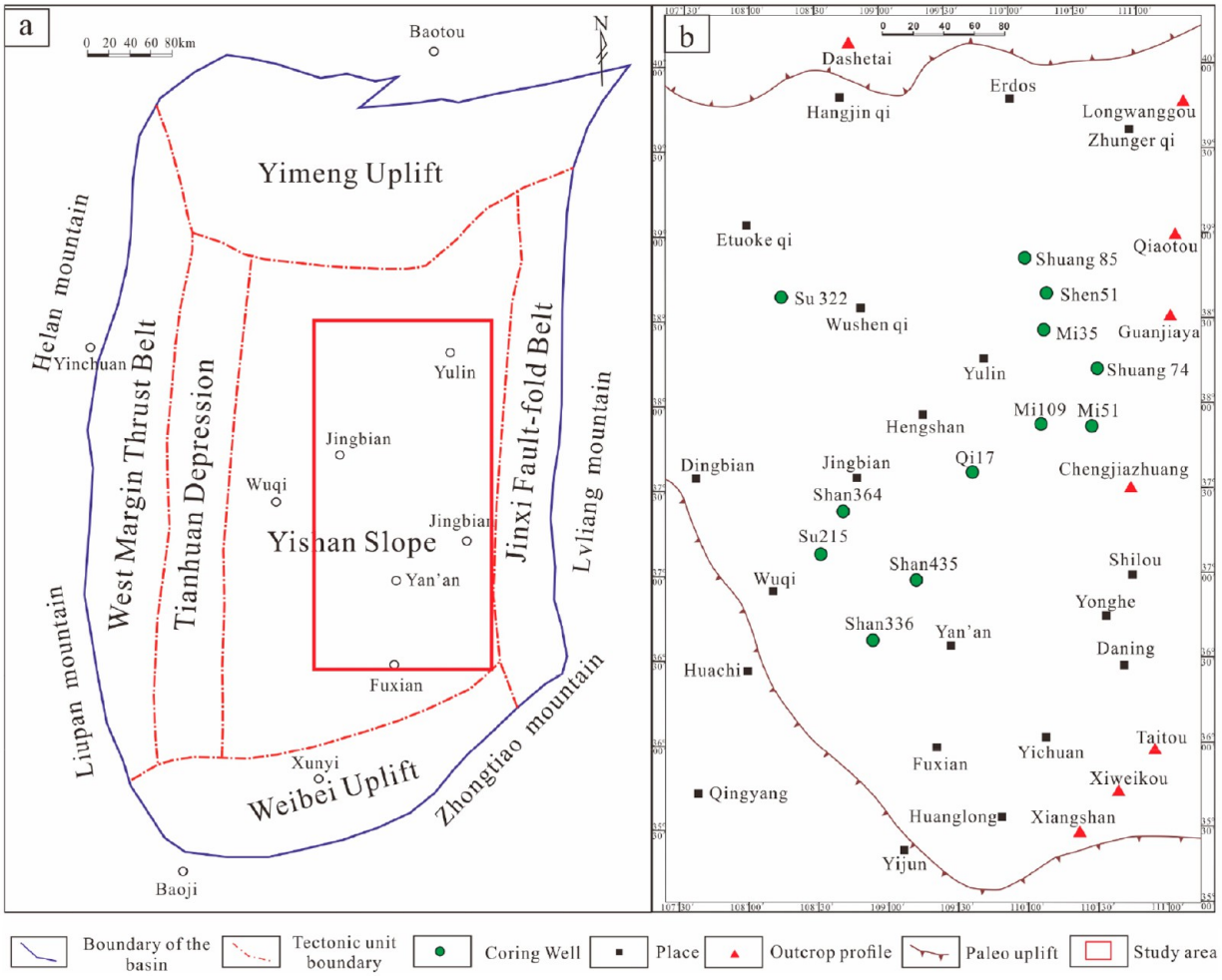

Figure 1. (a) Structural units of the Ordos Basin. (b) The location of Coring well.

related to the parameters.[13−15] Pore structure (pore size and shape, pore size distribution, and pore connectivity) is the most critical factor affecting the macroscopic reservoir quality (porosity and permeability). Therefore, it is necessary to study the pore structure of tight sandstone in coal measures. The experimental methods to characterize the pore structure include qualitative and quantitative methods.[13,14] Qualitative experimental methods include casting thin sections,[11−13,16] scanning electron microscopy,[10−14,16] and X-CT scanning technology,[17,18] which can directly study the geometry and distribution of pores (where casting thin sections and scanning electron microscopes provide two-dimensional spatial distribution and CT scanning provides three-dimensional spatial distribution). An optical microscope or scanning electron microscope can directly observe pore type and size; CT scanning technology carries the advantages of dynamic, quantitative, and nondestructive testing and has no special requirements for samples. Simultaneously, this technology can quantitatively analyze the nonuniformity of the internal pore structure of tight sandstone. The degree of homogeneity provides an excellent experimental platform to study the pores network of tight sandstone in coal measures. Quantitative experimental methods include mercury intrusion experiments (high-pressure mercury intrusion and rate-controlled mercury injection),[11] nuclear magnetic resonance,[11,19] and adsorption experiments (N_2 adsorption and CO_2 adsorption),[20] which can indirectly derive pore volume, specific volume, volume distribution, and other parameters. Compared with conventional natural gas reservoirs, tight sandstones in coal measures have more fine-grain sizes[21−23] and broader pore ranges.[13,14,17,23] The high-pressure mercury intrusion experiment can reveal the different pore size distributions (nano-micron). The CT scanning technology can reveal pores' three-dimensional spatial morphology without damaging the sample and provide morphological information regarding the pore network, including pore size, shape, connectivity, and distortion. Therefore, this paper will combine qualitative and quantitative research, including cast thin sections, scanning electron microscopy, physical property testing, high-pressure mercury intrusion, and CT scanning, to characterize the pore structure of tight sandstone in coal measure in both with two dimensions and three dimensions, ranging from nanometers to micrometres.

Tight sandstone in coal measures has the particularity of small pore throats (micron−nano scale), complex pore structure, and high heterogeneity.[17,23] The fractal theory is introduced to quantify the pore structure's irregularity, complexity, and heterogeneity based on the above experimental methods. The fractal dimension represents the irregularity and complexity of microscale structure[17,18] and can be obtained from data on N_2 adsorption,[20] high-pressure mercury intrusion,[7,19] rate-controlled mercury injection,[11] NMR,[11,18] and X-CT.[18]

https://dx.doi.org/10.1021/acs.energyfuels.0c03991
Energy Fuels 2021, 35, 3887−3898

In this paper, samples from different wells of tight sandstone in a coal-measure reservoir of Carboniferous Benxi Formation in the Ordos Basin were used to perform casting section, scanning electron microscopy, XRD, physical property testing, high-pressure mercury intrusion, and X-CT scanning experiments to determine pore types and pore throat characteristics. Simultaneously, the pore throat data of different scales obtained by the high-pressure mercury intrusion experiment were discussed in fractal theory to determine the relationship between the reservoir's micropore structure and the macroparameters (porosity, permeability) and to study the tightness of coal measures. Furthermore, we studied the internal pore structure and flowing-laws of sandstone gas reservoirs in tight coal measure and revealed the mechanism of oil and gas storage and seepage from a microscopic point of view to provide references for the efficient development of unconventional oil and gas resources.

2. GEOLOGICAL SETTING

The Ordos Basin is the second-largest sedimentary basin in China[25] with an area of 25×10^4 km^2 and developed based on the Archean-Paleoproterozoic crystalline basement.[26−29] The basin can be divided into six primary structural units: the Yimeng Uplift, Weibei Uplift, West Margin Thrust Belt, Tianhuan Depression, Yishan Slope, and Jinxi Fault-fold Belt (Figure 1a). The total natural gas resources are 15.16×10^{12} m^3, of which tight gas resources are 10.37×10^{12} m^3, accounting for about 68% of the total natural gas resources. At present, four tight gas fields with proven reserves of more than 100 billion m^3 have been discovered, including Sulige, Wushenqi, Daniudi, and Shenmu. The cumulative geological reserves of tight gas are about 3.53×10^{12} m^3, accounting for 84% of the total discovered natural gas reserves in the basin, revealing the abundant tight gas resources in the Ordos Basin.[26] The Benxi Formation in the Ordos Basin is a marine-continental transitional facies (Figure 2), of which the northern part is a tidal-controlled delta, and the south is a barrier island deposition-lagoon.[30] According to the lithological combination and sedimentary cycle characteristics, the Benxi Formation can be further subdivided into a Ben 3 member (B3), a Ben 2 member (B2), and a Ben 1 member (B1) from the bottom to the top.[26,30] The B3 member is mainly a set of gray, off-white bauxite, and bauxite mudstone; the lithology of the B2 member is a set of dark gray siltstone intercalated with off-white fine-coarse sandstone and limestone. The primary lithology of the B1 member is a set of sandstone, limestone, and coal seams.[26,30]

In this paper, the samples were all the most representative tight sandstone samples from the Carboniferous Benxi Formation in the eastern Ordos Basin, with well-location shown in Figure 1b.

3. EXPERIMENTAL METHOD AND FRACTAL MODEL

3.1. Experimental Method. Under the conditions of simulated formation overburden pressure (maximum pressure 70 MPa), detection temperature of 20 °C, and humidity of 37%, following the American Petroleum Institute standard (API RP-40), the PoroPDP-200 was used with the nonsteady-state method (pressure pulse attenuation method) to measure the permeability of 1350 samples,[10,13,14] and the Boyle's law was used to measure porosity,[8,13,14] thus obtaining the porosity and permeability in the study area.

Cast thin sections were made by injecting red- or blue-dyed resin into thin sections (155 pieces) that had been washed and evacuated,

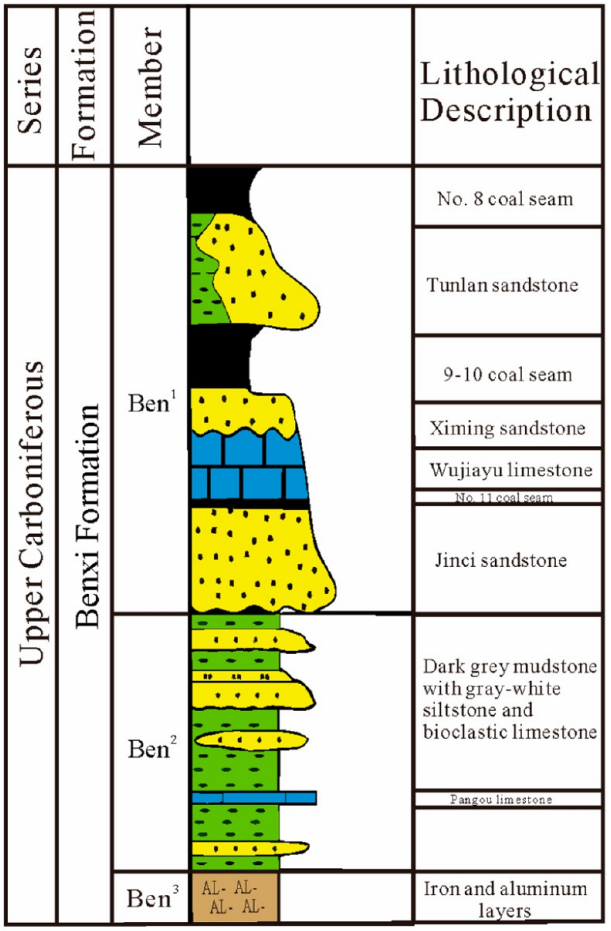

Figure 2. Lithological column of the Benxi Formation in the Ordos Basin.

and the skeleton particles were observed under the Leica optical microscope. The intergranular pores were filled with minerals and so was the pore throat system.[14,16] The scanning electron microscope used the AMETEK Quanta FEG400 energy spectrometer produced by the American EDAX company to observe the carbon coating on the freshly broken rock surface to determine the pore geometry, pore filling, lining, cement, and various minerals.[14,16,24] It was performed on 12 samples to determine the mineral compositions and their content according to the X-ray diffraction analysis method of clay minerals and common nonclay minerals in sedimentary rocks.

A PoreMaster-60 instrument was used on 14 samples in the study area to perform a high-pressure mercury intrusion experiment under continuous pressure (vacuum to 60 000 psi [415 MPa]) to characterize the complexity and heterogeneity of the pore throat structure[7] including pore size range, total pore volume, and pore surface area. The capillary model proposed by Washburn (1921)[31] gives the relationship between capillary pressure and pore throat radius. It can be expressed mathematically as the following:

$$P_c = \frac{2\sigma\cos\theta}{r}$$

where P_c is the capillary pressure (in MPa), σ is the interfacial tension (in N/m), θ is the wetting angle (in °), and r is the pore throat radius (in μm).

Three samples with a diameter of 2 mm were prepared for the CT scanning experiment.[32] The German general nano X-ray digital core analysis system (GE Phoenix Nanotom S) was adopted; the voltage was between 40 and 80 kv, the resolution was 0.2−0.35 μm, and the power was 1−5 W. The Phoenix Datosx 2 Acq X software of GE was used to reconstruct the scanned data's digital 3D model. Finally,

https://dx.doi.org/10.1021/acs.energyfuels.0c03991
Energy Fuels 2021, 35, 3887−3898

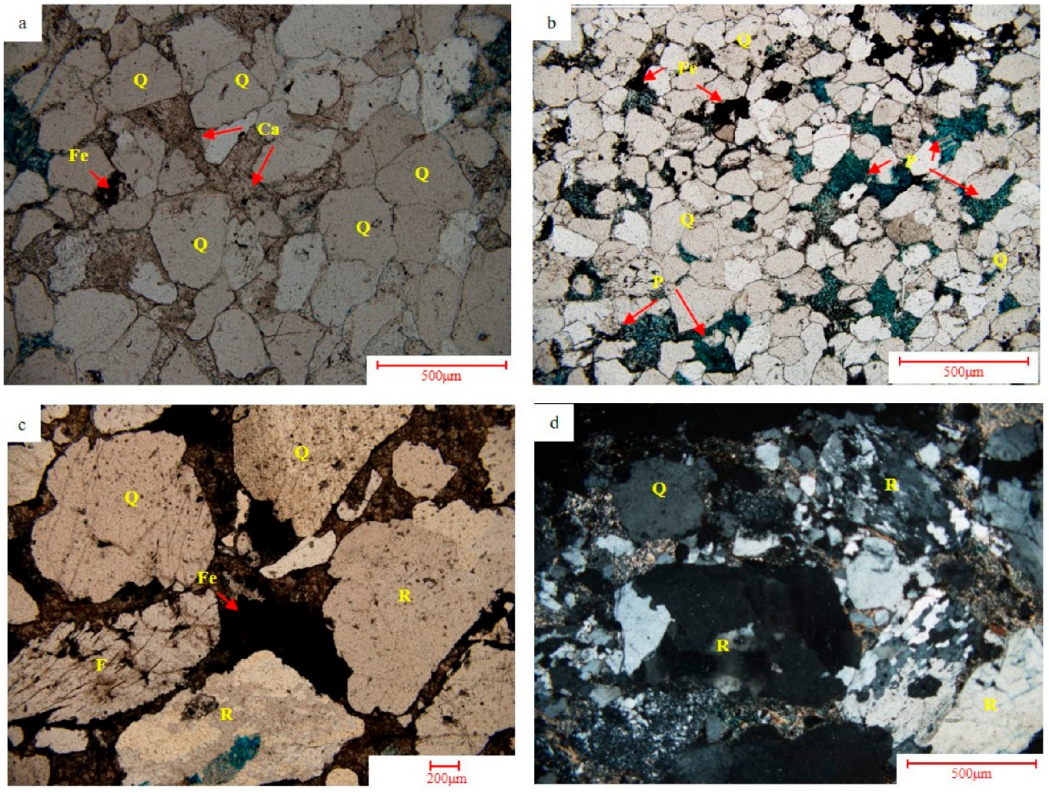

Figure 3. Microscopic observation showing petrographic characteristics, rock compositions, contact relationships, sorting, and roundness of various types of tight reservoirs in Benxi Formation. Q represents quartz content. F represents feldspar content. R represents lithic content. Ca represents calcite. Fe represents iron. P represents pores. (a) Quartz sandstone, the cement are calcite and iron between particles, line−concave−convex, Shan336, 3833.2 m. (b) Quartz sandstone, the grains are filled by authigenic quartz particles, the blue represents pores, mosaic contact, Shan 336, 3833.2 m. (c) Lithic quartz sandstone, the debris are mainly composed by feldspar and silica, point contact, Shan 468, 3176.9 m. (d) Lithic sandstone, the grains are filled by authigenic quartz particles and mud, line contact, Su 215, 3891.5 m (+).

Volume Graphics Studio Max and AVIZO 8.0 software were used to analyze and process the reconstructed 3D digital model, display 3D internal views, extract core pores, and analyze. The dark black area represents the pores in the sample, and the gray and white areas represent the rock matrix (white is a higher density material).

3.2. Fractal Theory. The fractal dimension is used for the quantitative characterization, classification, and evaluation of reservoirs. According to the principle of fractal geometry,[33−36] the fractal geometric formula of the pore size distribution was obtained.

$$\log S_w = \log(1 - S_{Hg}) = (3 - D)\log r - (3 - D)\log r_{max}$$

where D is the fractal dimension, and S_{Hg} is the mercury saturation, %; r_{max} is the maximum pore radius (in μm). S_w is the cumulative pore volume fraction (in %). The fractal dimension of porous rocks is usually 2−3. The closer it is to 2, the stronger the reservoir's homogeneity is, and the closer it is to 3, the more complex the reservoir's pore structure is.

4. RESULTS

4.1. Lithological Composition and Physical Characteristics. Observation under the microscopic shows that quartz sandstone (Figure 3a,b) and lithic quartz sandstone (Figure 3c) are the primary sandstone types of Benxi Formation, followed by lithic sandstone (Figures 3d and 4). Feldspar particles are almost completely eroded or replaced.[37] This high intensity of dissolution is due to acidic fluids resulted from hydrocarbon generation in coal measures.[9−11] In the Benxi Formation, ingredient maturities are high. The sorting is good−medium and the round is between subangular and subround. Particles are line−concave−convex.

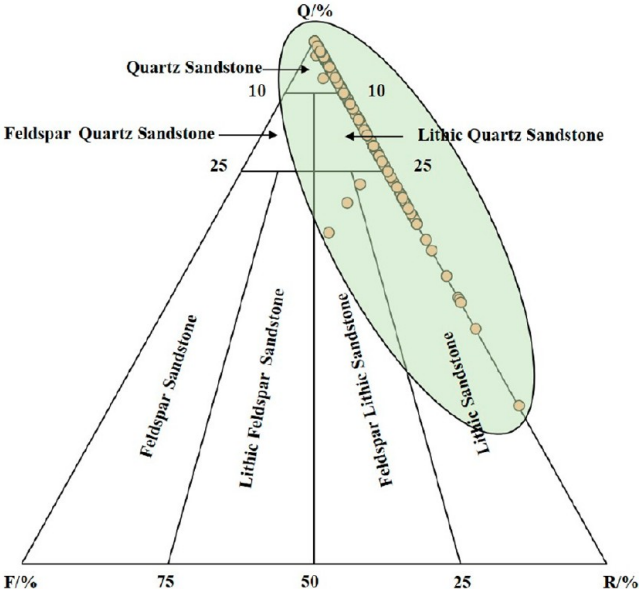

Figure 4. Characteristics of tight sandstone reservoir composition of Benxi Formation in Ordos Basin (280 samples). Q represents quartz content. F represents feldspar content. R represents lithic content. The data are almost distributed in the area of quartz sandstone, lithic quartz sandstone, and lithic sandstone. Only two samples are feldspar lithic sandstone. There is no feldspar quartz sandstone, feldspar sandstone, or lithic feldspar sandstone in the study area.

https://dx.doi.org/10.1021/acs.energyfuels.0c03991
Energy Fuels 2021, 35, 3887−3898

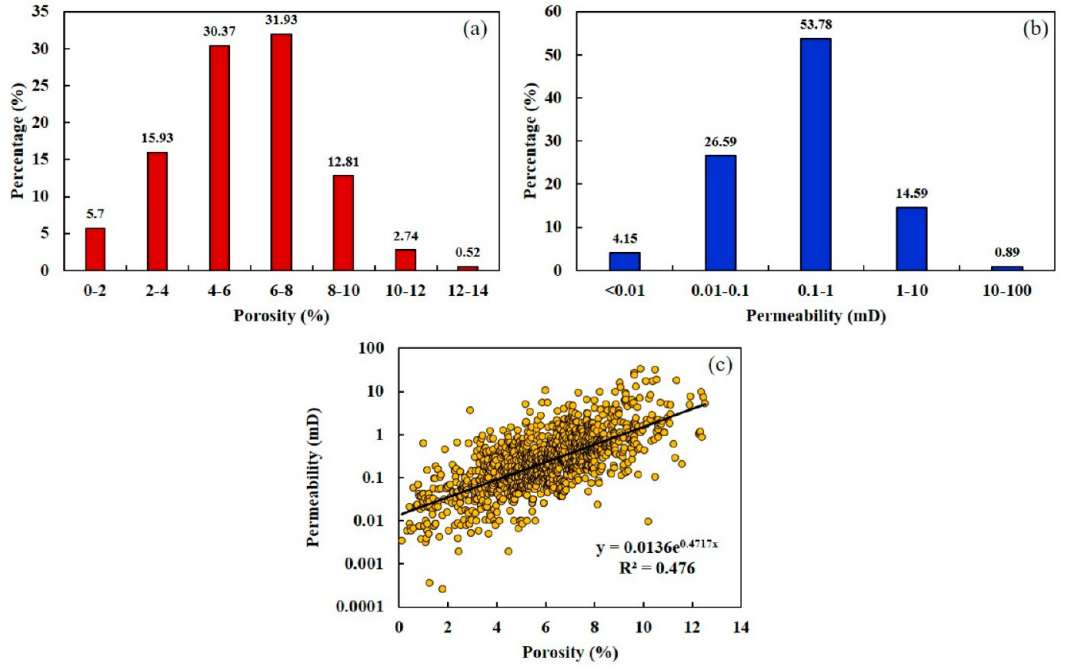

Figure 5. Porosity and permeability histogram and porosity and permeability scatter plot.

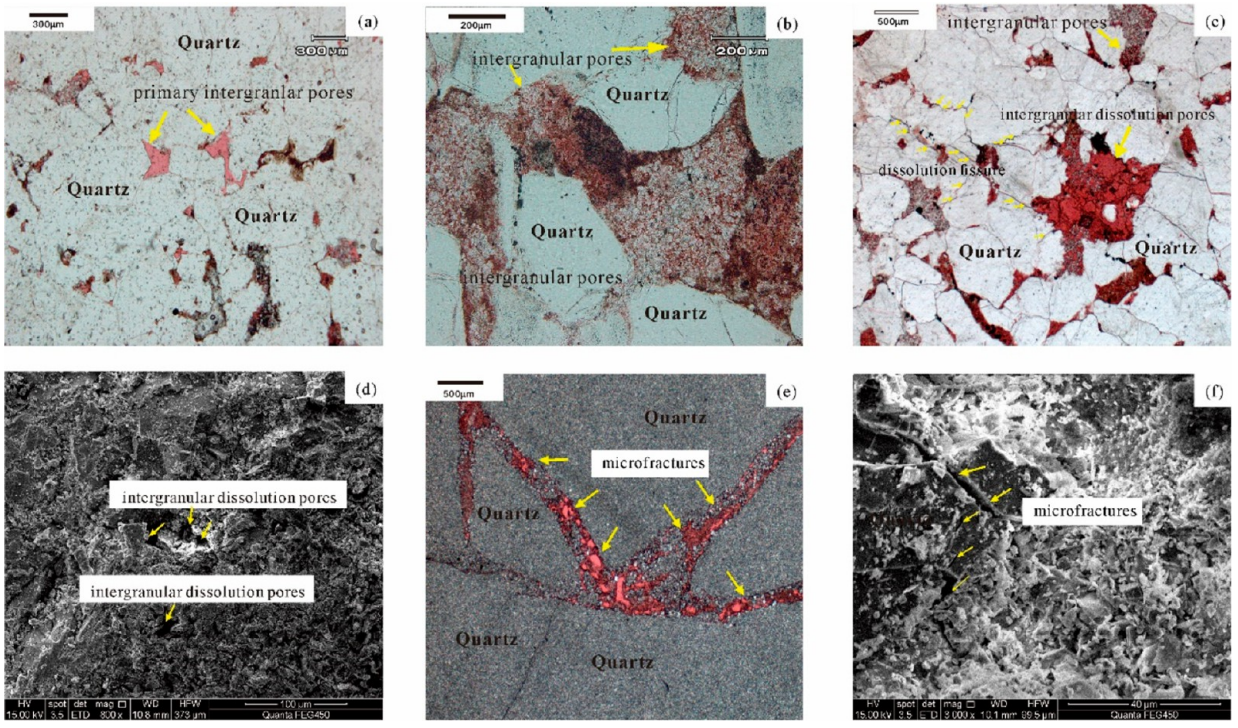

Figure 6. Thin section and scanning electron microscope image of tight sandstone in coal measure of Benxi Formation: (a) primary intergranular pores between quartz particles, (b) intergranular pores formed by clay minerals, (c) dissolution pores of harborlike, (d) intergranular dissolution pores between grains, (4) well-developed microfractures, and (f) microfractures between brittle minerals.

The Benxi Formation reservoir is a tight sandstone reservoir,[28,30] which has poor physical properties. The porosity varies from 0.12 to 12.53%, mostly located in the range 2−8%, with an average value of 5.85% (Figure 5a). The permeability ranges from 0.003 to 33.591 mD, mostly less than 1 mD, with an average value of 0.764 mD (Figure 5b). There is a certain positive relationship between the porosity and permeability of tight reservoirs (R^2 is 0.476) (Figure 5c), indicating that pores still dominate the reservoir space of the study area.

4.2. Pores Types and Characterization. It is found that secondary pores dominated the reservoir followed by the primary and microfractures, according to the cast thin sections and scanning electron microscope images.

The primary pores controlled by the compaction degree, the sediment debris structure, the sorting, and the content of the

https://dx.doi.org/10.1021/acs.energyfuels.0c03991
Energy Fuels 2021, 35, 3887−3898

Table 1. Pore Structure Parameters of the Research Samples Obtained From the High-Pressure Mercury Intrusion Experiment[a]

well	depth (m)	ϕ (%)	K (mD)	sorting	median radius (μm)	displacement pressure (MPa)	maximum mercury saturation (%)	efficiency of mercury withdrawal (%)
Shan 364	3981.7	7.7	2.278	0.72	0.644	0.347	94.8	57.994
Shuang 74	2132.5	5	1.101	1.86	0.454	0.4762	85.73	11.185
Su 322	3557.7	5.1	0.556	0.3	0.252	0.813	83.84	15.553
Shuang 85	2315.8	6.2	0.458	1.63	0.1097	0.8878	76.05	47.353
Shan 336	3841.2	3.8	0.283	0.21	0.308	1.148	88.87	7.113
Shuang 85	2317	6.7	0.364	1.51	0.0952	1.1547	85.58	52.962
Shan 336	3835	5.6	0.306	0.19	0.434	1.23	95.79	34.018
Shan 336	3836	3.7	1.935	0.17	0.31	1.445	92.88	45.05
Shan 336	3827.6	4.1	0.109	0.11	0.2	1.622	87.96	10.979
Shuang 74	2129.1	5.5	0.156	0.99	0.161	2.078	95.62	25.143
Shan 364	3975.8	4.6	0.106	0.09	0.156	2.455	91.23	18.582
Shan 364	3973	0.9	0.0242	0.07	/	2.63	38.02	8.824
Su322	3560.3	1.1	0.0351	0.07	/	3.02	44.075	16.279

[a]Green background = Type I formation. Orange background = Type II formation. Blue background = Type III formation. / = null value. ϕ = porosity, %. K = permeability, mD.

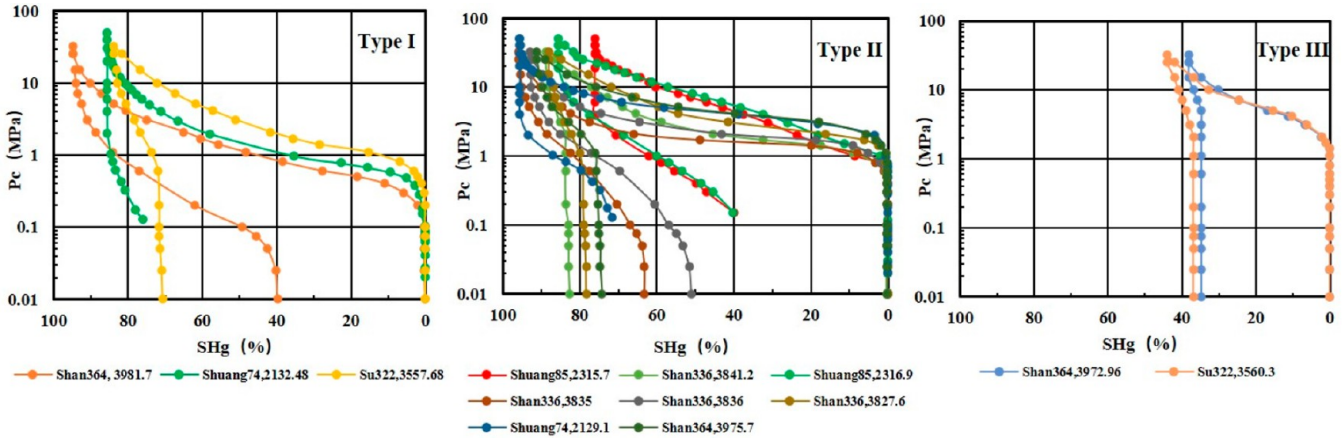

Figure 7. Different types of mercury injection curve.

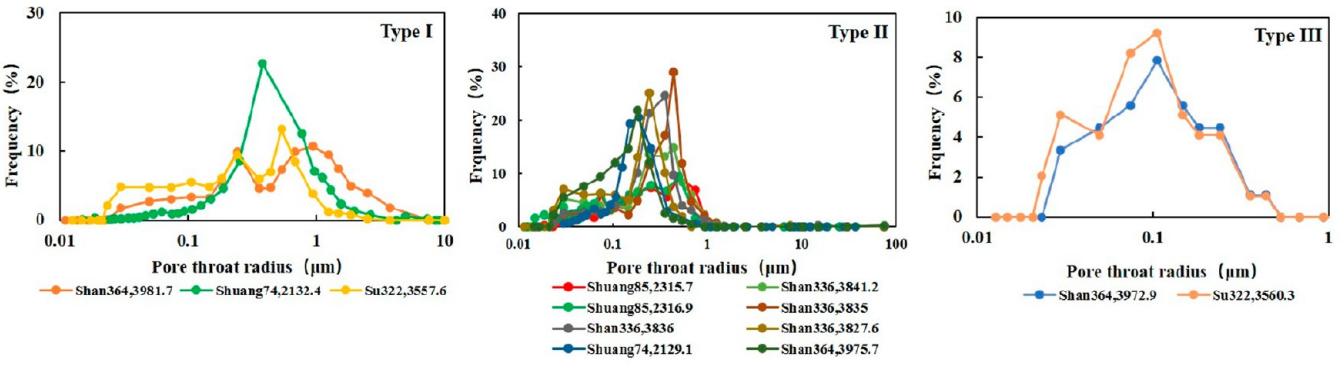

Figure 8. Pore size distribution chart of Benxi Formation.

miscellaneous base are mainly the remaining primary intergranular pores. The edges of the pore are mostly straight, triangular, or irregular polygons (Figure 6a). Secondary pores include three types of intergranular dissolved pores, intragranular dissolved pores, and intercrystalline pores (Figure 6b). The number of pores is relatively limited, and the porosity is small. Intergranular dissolution pores (Figure 6c,d) are mainly the pores distributed between particles formed by the dissolution of particle edges and particle cement and miscellaneous bases. Most of the pores are irregular and harborlike. The Benxi Formation contains almost no feldspar (content <1%) (Figure 4).[30,38] The intragranular dissolved pores are mainly debris dissolution pores shaped as isolated or honeycomb. Dissolution intergranular pores are mainly between kaolinite cement (kaolinite-dissolved intercrystalline pores) (Figure 6b). These pores are fine and mostly honeycomb or spotted, controlled by the types and degree of cementation. Microfractures (Figure 6e,f) are highly common in the study area. They are long, irregular strips with good connectivity and long extension distances. They can effectively

https://dx.doi.org/10.1021/acs.energyfuels.0c03991
Energy Fuels 2021, 35, 3887−3898

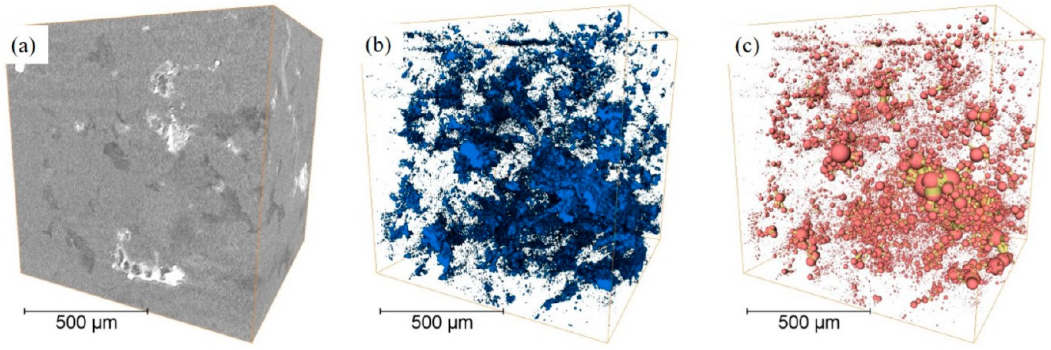

Figure 9. Three-dimensional CT images of Qi17. (a) Three-dimensional CT image of the sample. (b) Three-dimensional pore structure model. (c) Three-dimensional pore throat network model. The pink balls in the pore throat network model represent pores, and the yellow rods represent throats.

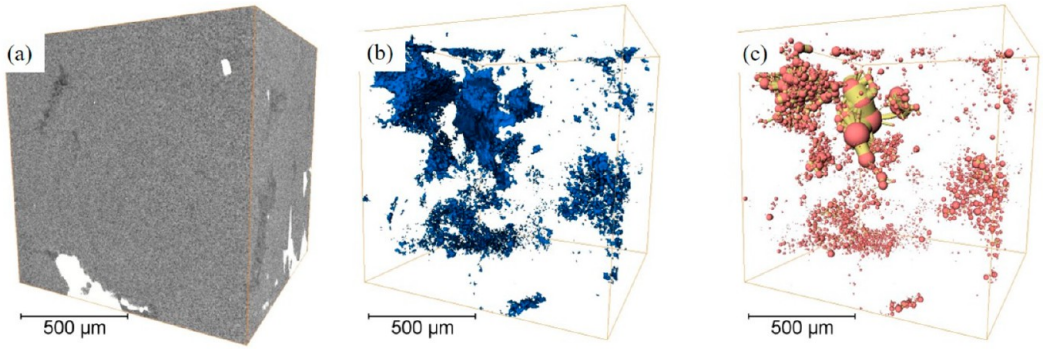

Figure 10. Three-dimensional CT images of Shan 336. (a) Three-dimensional CT image of the sample. (b) Three-dimensional pore structure model. (c) Three-dimensional pore throat network model. The pink balls in the pore throat network model represent pores, and the yellow rods represent throats.

Table 2. Data Table of Core CT Test Results

reservoir type	well	depth	average pore radius/ μm	porosity quantity	porosity volume/ μm^3	average length of throat/ μm	percentage of connected volume/%
I	Qi17	3027	1.055	20 603	367 853.312	10.216	35.028
II	Shan 336	3835	1.184	24 416	2 510 780.824	40.976	89.579

drain oil and gas and are virtual storage spaces and migration channels for oil and gas.

4.3. Pore Throat Size Distribution. *4.3.1. High-Pressure Mercury Intrusion Tests.* The parameters of pore throat morphology of the Benxi Formation were obtained on 13 samples of tight reservoirs in the Benxi Formation through high-pressure mercury intrusion experiments (Table 1).[24,39] The core samples were divided into three types based on curve shape and drainage pressure (Figure 7).

The drainage pressure of type I reservoirs is generally less than 1 MPa, ranging from 0.347 to 0.813 MPa, with an average of 0.545 MPa. Type II displacement pressure is concentrated between 1 and 2 MPa, with an average of 1.502 MPa. Type III has the highest displacement pressures, which are all greater than 2 MPa. It can be seen that, compared to Type II and Type III reservoirs, Type I reservoirs have the largest pore throat radius and better porosity and permeability and are more conducive to gas filling. The slopes of type I and type II mercury curves are longer and gentler, which means that the two types are better separated.

At present, the most commonly used pore size classification is IUPAC in unconventional shale reservoirs, and the main focus of this paper is tight sandstone. According to the size and type of pores, selecting pore classification standard from Xoaoth (1966),[40] the pores can be divided into small pores (<0.1 μm), mesopores (0.1−1 μm), and macropores (>1 μm) (Figure 8). Overall, the pore throat radii of the tight sandstone reservoirs of the Benxi Formation range from 0.01 to 7.282 μm. Type I formation is characterized by a predominant peak at pore size of 0.38 μm, resulting in a monomodal PSD shape in the relatively large pore size range (from 0.015 to 7.282 μm, average 1.02 μm). Type II formation presents both monomodal and bimodal PSD shape, while pores with size from 0.3 to 0.84 μm dominate the pore space (average 0.54 μm). The PSD of type III formation is typical bimodal shaped with peaks at 0.02 and 0.1 μm, respectively. Pores, sized from 0.023 to 0.441 μm dominate the pore network of type III formation.

From the pore size's perspective, type I formation is the best out of the three, while type III formation is the least best one for petroleum charging and accumulation. Also, it is worth noting that mesopores and macropores are highly developed, while micropores are rarely developed.

4.3.2. High-Resolution Microcomputed Tomography. Two samples were selected for X-CT scanning. The pore throat system connected by the tight sandstone of the coal

https://dx.doi.org/10.1021/acs.energyfuels.0c03991
Energy Fuels 2021, 35, 3887−3898

measures of the Benxi Formation is mainly composed of a micropore throat system (Figures 9 and 10), and a complex pore throat network composed of multiple independent connected pore throat systems is developed,[34] which provides oil and gas flow channels according to the results of micron CT scanning. According to the curved shape and displacement pressure of high-pressure mercury injection,[41] Qi17 is a type I reservoir with a total of 20 603 pores and a pore volume of 367 853.312 μm^3 (Table 2); Shan 336 is a type II with a total of 24 416 pores. The pore volume is 2 510 780.824 μm^3, and the connected volume percentage is 35%. The pores are relatively developed, the average length of the throat reaches 40.976 μm, and the connected volume percentage is as high as 89.6% (Table 2).

4.4. Fractal Dimension Characteristics. The double logarithmic coordinates exhibit a significant linear relationship, indicating that the Benxi Formation coal-measures' tight sandstone samples have fractal characteristics and can be characterized by fractal theory.[34] If they have fractal characteristics, the two double logarithmic coordinates will show a significant linear relationship; otherwise, it is understood that they do not have fractal characteristics. According to the mercury saturation and pore radius obtained by the high-pressure mercury injection, in the scatter plot of lg (1-S_{Hg}) and lgr,[42] there are two obvious turning points in the relationship graph between (Figure 11). According to these two obvious

$$D = \frac{D_1 \times \varphi_1 + D_2 \times \varphi_2 + D_3 \times \varphi_3}{\varphi_1 + \varphi_2 + \varphi_3}$$

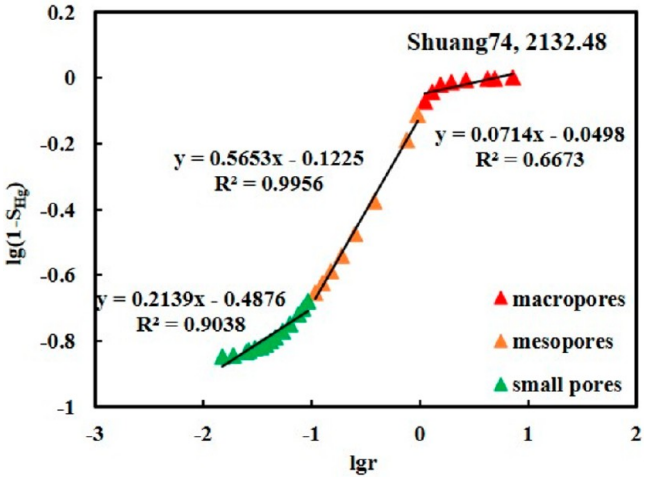

Figure 11. Fractal analysis for heterogeneity interpretation of pore network, taking sample Shuang 74 as an example.

turning points, the fractal dimensions D_1, D_2, and D_3 corresponding to small pores, mesopores, and macropores are calculated (Tables 3 and 4). The total fractal dimension D of the entire pore space is obtained by the pore weighted average as

$$D = \frac{D_1 \times \varphi_1 + D_2 \times \varphi_2 + D_3 \times \varphi_3}{\varphi_1 + \varphi_2 + \varphi_3}$$

5. DISCUSSION

5.1. Pore Structure and Fractal Dimension Analysis. From the high-pressure mercury injection curve obtained in Figure 7 and the displacement pressure obtained in Table 1, Type I reservoirs show the highest quality, which is more conducive to gas filling and enrichment;[42,43] Type II shows the middle quality, and Type III is the worst quality. The porosity and permeability of Type I tight sandstone reservoirs of the Benxi Formation coal measures are both the highest, as classified through the high-pressure mercury intrusion.[7,8] Type III reservoirs have the worst physical properties. However, the actual physical property test found that the porosity of Qi17 (type I reservoir) is higher than that of Shan 336 (type II), which fulfills the classification standard of high-pressure mercury intrusion, but the permeability of Qi17 is lower than that of Shan 336. It is contrary to the conclusion drawn by the high-pressure mercury intrusion experiment.

We tried to analyze the data of different pores' contribution rate to explain the contradiction caused by the above-mentioned high-pressure mercury intrusion curve classification (small pores, mesopores, and large pores) and the corresponding fractal dimension (Tables 3 and 4). Because the physical properties of Type III reservoirs fulfill the classification criteria for high-pressure mercury intrusion, this article focuses on analyzing the reasons for the high porosity and low permeability of Type I reservoirs or the low porosity and high permeability of Type II reservoirs. From Figure 12, it can be deduced that the total fractal dimension and porosity have a weak negative correlation and that, as the total fractal dimension increases, the permeability also increases. It can be explained that the larger the total fractal dimension is, the stronger the heterogeneity of the reservoir is,[8] which means that, with more complexity of the pore structure, the porosity decreases and permeability increases.

We created scatter plots of the porosity of small pores, mesopores, and macropores and their corresponding fractal dimension.[42,44] As shown in Figure 13, the correlation between the fractal dimension and mesopores and macropores is obvious, and the correlation with small pores is very weak. It shows that mesopores and macropores have a more significant influence on porosity, and the fractal dimensions of mesopores and macropores have a better correlation with their corresponding porosity. With the increase of the fractal dimension, mesopore and macropore corresponding porosities shows a decreasing trend, indicating that the contribution rate of mesopores and macropores to porosity is more affected by heterogeneity. The permeability of small pores and mesopores has a weak correlation with their corresponding fractal dimensions. In contrast, macropores' permeability has an apparent negative correlation with their corresponding fractal dimensions, indicating that the influence of heterogeneity on the seepage of large pores is stronger than that of mesopores and micropores.[45]

Through a series of scatter plots of pore structure (sorting coefficient, maximum pore throat radius, and median radius) and reservoir physical properties (Figure 14), it can be seen that as the fractal dimension of macropores increases, the sorting coefficient decreases, and the better the sorting is, the better the storage and lesser the heterogeneity of the layer are.[46] Simultaneously, macropores' fractal dimension has the most apparent influence over the median radius and the maximum pore throat radius, indicating that macropores are the main contributor to the effective seepage storage space.[45,46]

5.2. Heterogeneity on Permeability. Through the curve obtained by the high-pressure mercury intrusion experiment (Figures 7 and 8) and the fractal dimension derived from the test results analysis (Tables 3 and 4), we can infer that the

https://dx.doi.org/10.1021/acs.energyfuels.0c03991
Energy Fuels 2021, 35, 3887−3898

Table 3. Fractal Dimension and Correlation Coefficient of Pores at Different Scales[a]

		macropore		mesopore		small pore	
well	depth (m)	D_3	R_3	D_2	R_2	D_1	R_1
Shan 364	3981.7	2.9402	0.544	2.2578	0.9926	2.445	0.9469
Shuang 74	2132.5	2.9286	0.6673	2.4347	0.9956	2.7861	0.9038
Su 322	3557.7	2.9942	0.4793	2.511	0.9974	2.5322	0.9997
Shuang 85	2315.8	2.9998	0.1587	2.6922	0.9881	2.5579	0.9571
Shan 336	3841.2	2.9995	0.1692	2.3449	0.9797	2.3675	0.9973
Shuang 85	2317	/	/	2.7073	0.9784	2.2875	0.9913
Shan 336	3835	2.9984	0.4418	1.9159	0.9655	2.272	0.9993
Shan 336	3836	2.9988	0.5226	2.0428	0.9521	2.4647	0.9916
Shan 336	3827.6	2.9989	0.7167	2.4385	0.9229	2.2662	0.994
Shuang 74	2129.1	/	/	2.4014	0.7818	2.05	0.9228
Shan 364	3975.8	/	/	2.5055	0.8143	2.1335	0.999
Shan 364	3973	/	/	2.8755	0.8355	2.8705	0.9825
Su 322	3560.3	/	/	2.8801	0.8121	2.8398	0.9996

[a]D represents the Fractal dimension. R represents correlation coefficient. / represents null value.

Table 4. Contribution of Different Pore Sizes to Porosity and Permeability[a]

		small pore		mesopore		macropore	
well	depth (m)	φ_1	K_1	φ_2	K_2	φ_3	K_3
Shan 364	3981.7	0.34	0.1022	3.75	1.1107	2.13	0.633
Shuang 74	2132.5	0.33	0.0596	2.75	0.4967	0.78	0.1413
Su 322	3557.7	0.59	0.0649	3.07	0.3357	0.16	0.018
Shuang 85	2315.8	1.34	0.0993	3.06	0.2264	0.01	0.0014
Shan 336	3841.2	0.42	0.032	2.65	0.1975	0.02	0.0016
Shuang 85	2317	2.32	0.1265	3.16	0.172	/	/
Shan 336	3835	0.3	0.0168	4.75	0.2596	0.05	0.0032
Shan 336	3836	0.21	0.0556	3.03	0.7672	0.03	0.0079
Shan 336	3827.6	0.66	0.0176	2.66	0.0709	0.02	0.0006
Shan 74	2129.1	0.91	0.026	4.11	0.1168	/	/
Shan 364	3975.8	0.7	0.0163	3.04	0.0702	0.01	0.0002
Shan 364	3973	0.07	0.0019	0.22	0.006	/	/
Su 322	3560.3	0.12	0.004	0.27	0.0086	/	/

[a]Green background = Type I formation. Orange background = Type II formation. Blue background = Type III formation. / = null value. ϕ = porosity, %. K = permeability, mD.

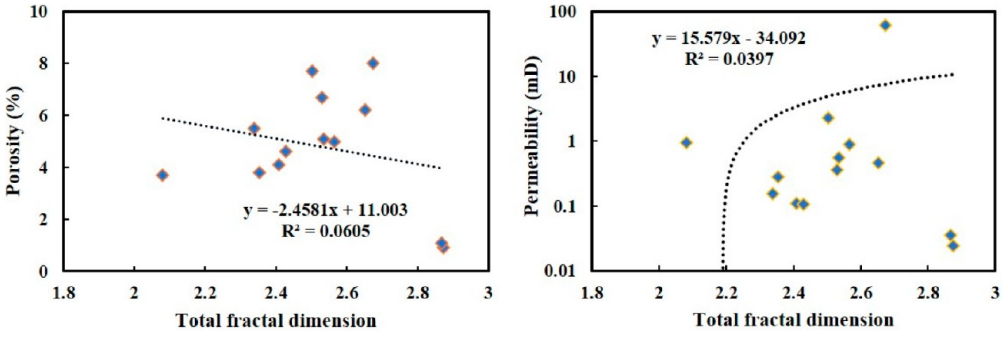

Figure 12. Relationship between total fractal dimension and porosity and permeability.

reason for the high porosity and low permeability of the tight reservoirs in coal measures of Benxi Formation is heterogeneity.[10,11,16] So, this section attempts to explore how heterogeneity affects the seepage of the study area, or in other words, what factors moderate the effectiveness of seepage.

Because high-pressure mercury injection cannot display the three-dimensional shape of pore space, the micro-CT experiment is used to observe the pore structure's complexity. The above micro-CT experiment results and data show that the average pore radius of Qi17 (Type I) and Shan 336 (Type II) are approximately the same. The pore volume of Qi17 is 367 853.312 μm^3, and that of Shan 336 is 2 510 780.824 μm^3. The differences in pore volume are nearly an order of magnitude, which shows that the tight sandstone reservoirs of the Benxi Formation have a strong heterogeneity and complex pore structure.[10,11,28,30] From the statistical average length of the throat, Shan 336 is 40.8 μm, while Qi17's throat is four times the average length; Shan 336 has a pore-to-throat connectivity ratio of over 89.5%, while Qi17 has a ratio of only

https://dx.doi.org/10.1021/acs.energyfuels.0c03991
Energy Fuels 2021, 35, 3887−3898

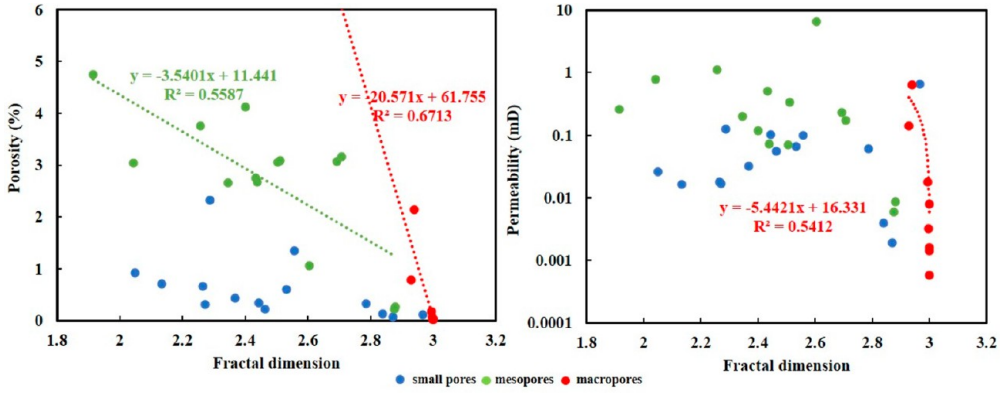

Figure 13. Relationship between fractal dimension and reservoir quality.

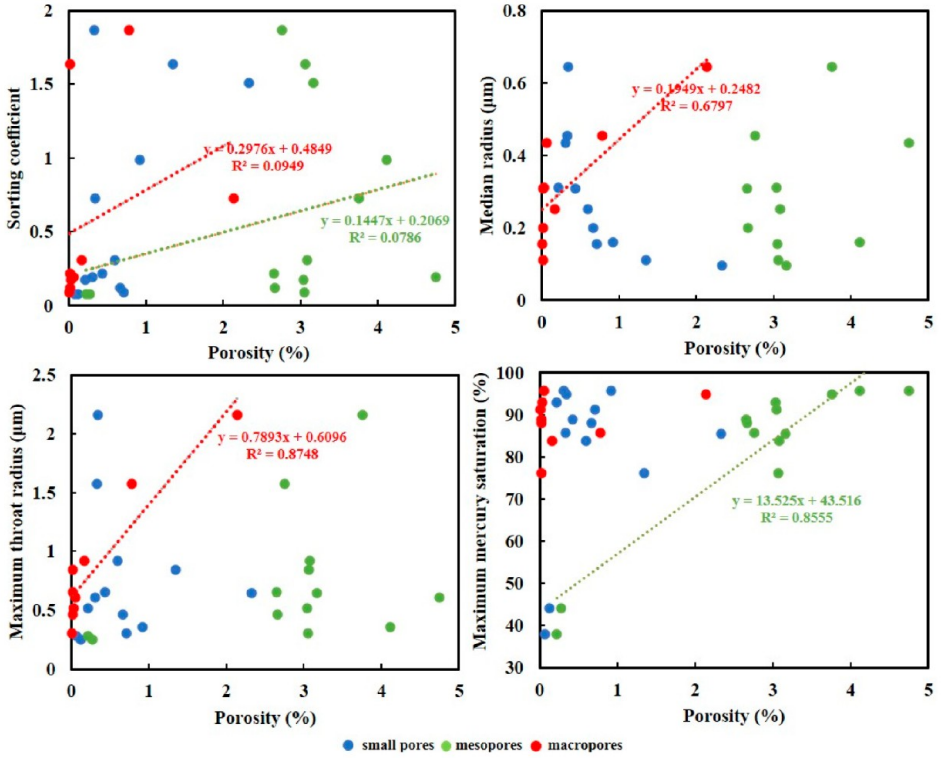

Figure 14. Influence of pore structure on reservoir quality.

Table 5. Identification of Whole-Rock Clay Minerals

well	depth (m)	quartz (%)	feldspar (%)	iron-containing dolomite (%)	siderite (%)	pyrite (%)	clay minerals (%)
Qi 17	3027	74.3	/	/	0.3	1.3	24
Shan 336	3835	91.7	/	0.6	/	2.6	5.1

35%. It can be seen that, under similar pore conditions, the average length of the second type reservoir's throat is longer, and the percentage of the connected volume of the throat is higher, leading to the low permeability of type I and high permeability of type II.

Clay minerals in tight reservoirs can divide large pores into small pores, block thick throats into thin throats, block pore–throat spaces, reduce pore volume, worsen throat connectivity, and reduce reservoir seepage capacity. The XRD data results show (Table 5) that the clay mineral content of Qi17 is 24%, which is much higher than that of Shan 336. It can be seen that the clay content of Type I reservoirs is higher than that of Type II, and the seepage capacity of reservoirs will be relatively weak. On the other hand, through the observation of cast thin sections and scanning electron microscopy, we found that kaolinite intercrystalline pores dominate the secondary dissolution pores of the Benxi Formation. There are two primary formation mechanisms for kaolinite. One is the transformation of clay-like substances carried by the parent rock during the diagenesis process, and the other is the dissolution of unstable minerals (mica, feldspar) by acidic fluids in the pore space. While clay minerals weaken the seepage capacity and destroy the reservoir's pore throat's pore throat, they can also restore part of the reservoir's seepage

https://dx.doi.org/10.1021/acs.energyfuels.0c03991
Energy Fuels 2021, 35, 3887−3898

capacity. In this paper, we discovered that clay minerals are relatively more destructive to Type I reservoirs. Therefore, the pore structure of Type II reservoirs is more conducive to hydrocarbon charging and accumulation.

6. CONCLUSION

Using high-pressure mercury intrusion and X-CT scanning technology, supplemented by fractal analysis, we characterized the pore structure of coal-measure tight sandstone reservoirs in coal measure. The conclusions are as follows:

(1) The type of pores is dominated by secondary pores, followed by primary pores and microcracks. There are pores of various sizes, of which medium and large pores are the main ones, followed by small pores. Small pores, mesopores, and macropores are developed in Type I reservoirs; mesopores and macropores are developed in Type II reservoirs, and macropores are poorly developed in Type III reservoirs.

(2) The contribution rate of mesopores and macropores to porosity is more affected by heterogeneity. With the increase of macropore fractal dimension D_3, the smaller the sorting coefficient is, the better the sorting and the reservoir's heterogeneity are. At the same time, D_3 has the most apparent influence over the median radius and maximum pore throat radius, indicating that macropores are the main contributor to the effective seepage storage space.

(3) Reservoir types obtained by high-pressure mercury injection show that the quality of type I reservoirs' quality is not necessarily better than that of type II. Type I reservoirs have the best porosity and minimum heterogeneity. Although Type II reservoirs have stronger heterogeneity than Type I, they have higher permeability.

(4) Under the same porosity conditions, the reservoir seepage is mainly determined by the throat radius and throat connectivity ratio. The larger the throat radius is, the higher the connection ratio and the stronger the seepage capacity are. As the content of clay minerals increases, the reservoir's heterogeneity increases, while the permeability capacity decreases.

AUTHOR INFORMATION

Corresponding Authors

Fujie Jiang − *State Key Laboratory of Petroleum Resources and Prospecting and College of Geoscience, China University of Petroleum, Beijing 102249, China; State Key Laboratory of Shale Oil and Gas Enrichment Mechanisms and Effective Development, SINOPEC, Wuxi 214162, China;* orcid.org/0000-0002-0089-2972; Email: jfjhtb@163.com

Zezhang Song − *State Key Laboratory of Petroleum Resources and Prospecting and College of Geoscience, China University of Petroleum, Beijing 102249, China; State Key Laboratory of Shale Oil and Gas Enrichment Mechanisms and Effective Development, SINOPEC, Wuxi 214162, China;* orcid.org/0000-0001-5573-1490; Email: songzz@cup.edu.cn

Authors

Jingyi Wang − *State Key Laboratory of Petroleum Resources and Prospecting and College of Geoscience, China University of Petroleum, Beijing 102249, China; State Key Laboratory of Shale Oil and Gas Enrichment Mechanisms and Effective Development, SINOPEC, Wuxi 214162, China*

Chunlin Zhang − *Research Institute of Petroleum Exploration & Development, PetroChina, Langfang 065000, China*

Wuling Mo − *Research Institute of Petroleum Exploration & Development, PetroChina, Langfang 065000, China*

Complete contact information is available at: https://pubs.acs.org/10.1021/acs.energyfuels.0c03991

Author Contributions

The manuscript was written through the contributions of all authors. All authors have given approval to the final version of the manuscript.

Notes

The authors declare no competing financial interest.

ACKNOWLEDGMENTS

This research was financially supported by the National Science and Technology Major Project (Grant No. 2017YFC0603106), the Major Technology Project of China Petroleum (Grant No. 2019B-0606), the National Key R&D Program of China (Grant No. 2016ZX05007-003), the Youth Program of the National Natural Science Foundation of China (Grant No.41802148), and the State Key Laboratory of Petroleum Resources and Prospecting (Grant No. 2462017YJRC025, Grant No. PRP/indep-04-1611). We would also thank the Langfang Branch of the PetroChina Exploration and Development Research Institute for providing core samples and necessary data. Constructive comments and suggestions from Wu Hao of Lanzhou University are much appreciated.

REFERENCES

(1) Zou, C.; Zhu, R.; Liu, K.; Su, L.; Bai, B.; Zhang, X.; Yuan, X.; Wang, J. Tight gas sandstone reservoirs in China: characteristics and recognition criteria. *J. Pet. Sci. Eng.* **2012**, *88*−*89*, 82−91.

(2) Hu, T.; Pang, X.; Jiang, S.; et al. Oil content evaluation of lacustrine organic-rich shale with strong heterogeneity: A case study of the Middle Permian Lucaogou Formation in Jimusaer Sag, Junggar Basin, NW China. *Fuel* **2018**, *221*, 196−205.

(3) Hu, T.; Pang, X.; Jiang, S.; et al. Impact of Paleosalinity, Dilution, Redox, and Paleoproductivity on Organic Matter Enrichment in a Saline Lacustrine Rift Basin: A Case Study of Paleogene Organic-Rich Shale in Dongpu Depression, Bohai Bay Basin, Eastern China. *Energy Fuels* **2018**, *32* (4), 5045−5061.

(4) Hu, T.; Pang, X.; Yu, S.; Wang, X.; Pang, H. Hydrocarbon generation and expulsion characteristics of Lower Permian P1f source rocks in the Fengcheng area, northwest margin, Junggar Basin, NW China: implications for tight oil accumulation potential assessment. *Geol. J.* **2016**, *51*, 800−900.

(5) Zou, C.; Guo, J.; Jia, A.; Wei, Y.; Yan, H.; Jia, C.; Tang, H. Connotations of scientific development of giant gas fields in China. *Nat. Gas Ind. B* **2020**, *7* (5), 533−546.

(6) Zhao, J.; Cao, Q.; Bai, Y.; Er, C.; Li, J.; Wu, W.; Shen, W. Petroleum accumulation from continuous discontinuous: concept, classification and distribution. *Acta Pet. Sin.* **2016**, *37* (2), 145−159.

(7) Song, Z.; Liu, G.; Yang, W.; Zou, H.; Sun, M.; Wang, X. Multifractal distribution analysis for pore structure characterisation of tight sandstone—A case study of the Upper Paleozoic tight formations in the Longdong District, Ordos Basin. *Mar. Pet. Geol.* **2018**, *92*, 842−854.

(8) Li, P.; Zheng, M.; Bi, H.; Wu, S.; Wang, X. Pore throat structure and fractal characteristics of tight oil sandstone: A case study in the Ordos Basin, China. *J. Pet. Sci. Eng.* **2017**, *149*, 665−674.

(9) He, M.; Huang, W.; Wang, Y.; Wang, Y.; Yan, D. *Res. Indus.* **2018**, *20* (2), 34−40.
(10) Wu, H.; Ji, Y.; Liu, R.; Zhang, C.; Chen, S. Insight into the pore structure of tight gas sandstones: a case study in the ordos basin, NW China. *Energy Fuels* **2017**, *31* (12), 13159−13178.
(11) Wu, H.; Zhang, C.; Ji, Y.; Liu, R.; Wu, H.; Zhang, Y.; Yang, J. An improved method of characterising the pore structure in tight oil reservoirs: Integrated NMR and constant-rate-controlled porosimetry data. *J. Pet. Sci. Eng.* **2018**, *166*, 778−796.
(12) Niu, X.; Cao, D.; Xu, H. Characteristics and control factors of tight sandstone reservoirs in marine-continental transitional coal measures. *Coal Sci. Tech.* **2018**, *46* (4), 188−195.
(13) Clarkson, C. R.; Freeman, M.; He, L.; Agamalian, M.; Melnichenko, Y. B.; Mastalerz, M.; Blach, T. P. Characterization of tight gas reservoir pore structure using USANS/SANS and gas adsorption analysis. *Fuel* **2012**, *95*, 371−385.
(14) Clarkson, C. R.; Solano, N.; Bustin, R. M.; Bustin, A. M. M.; Chalmers, G. R. L.; He, L.; Blach, T. P. Pore structure characterisation of North American shale gas reservoirs using USANS/SANS, gas adsorption, and mercury intrusion. *Fuel* **2013**, *103*, 606−616.
(15) Mehmani, A.; Mehmani, Y.; Prodanović, M.; Balhoff, M. A forward analysis on the applicability of tracer breakthrough profiles in revealing the pore structure of tight gas sandstone and carbonate rocks. *Water Resour. Res.* **2015**, *51* (6), 4751−4767.
(16) Shao, X.; Pang, X.; Jiang, F.; Li, L.; Huyan, Y.; Zheng, D. Reservoir characterisation of tight sandstones using nuclear magnetic resonance and incremental pressure mercury injection experiments: implication for tight sand gas reservoir quality. *Energy Fuels* **2017**, *31* (10), 10420−10431.
(17) Hou, X.; Zhu, Y.; Chen, S.; Wang, Y.; Liu, Y. Investigation on pore structure and multifractal of tight sandstone reservoirs in coal bearing strata using LF-NMR measurements. *J. Pet. Sci. Eng.* **2020**, *187*, 106757.
(18) Zhang, K.; Lai, J.; Bai, G.; Pang, X.; Ma, X.; Qin, Z.; Fan, X. Comparison of fractal models using NMR and CT analysis in low permeability sandstones. *Mar. Pet. Geol.* **2019**, 104069.
(19) Lai, J.; Wang, G.; Fan, Z.; Chen, J.; Wang, S.; Zhou, Z.; Fan, X. Insight into the pore structure of tight sandstones using NMR and HPMI measurements. *Energy Fuels* **2016**, *30* (12), 10200−10214.
(20) Jiang, F.; Chen, D.; Chen, J.; Li, Q.; Liu, Y.; Shao, X.; Hu, T.; Dai, J. Fractal analysis of shale pore structure of continental gas shale reservoir in the Ordos Basin, NW China. *Energy Fuels* **2016**, *30* (6), 4676−4689.
(21) Zhao, P.; Wang, Z.; Sun, Z.; Cai, J.; Wang, L. Investigation on the pore structure and multifractal characteristics of tight oil reservoirs using NMR measurements: Permian Lucaogou Formation in Jimusaer Sag, Junggar Basin. *Mar. Pet. Geol.* **2017**, *86*, 1067−1081.
(22) Li, J.; Guo, B.; Zheng, M. Main types, geological features and resource potential of tight sandstone gas in China. *Nat. Gas Geol.* **2012**, *23* (4), 607−615.
(23) Zhao, Y.; Sun, Y.; Liu, S.; Chen, Z.; Yuan, L. Pore structure characterisation of coal by synchrotron radiation nano-CT. *Fuel* **2018**, *215*, 102−110.
(24) Lai, J.; Wang, G. Fractal analysis of tight gas sandstones using high-pressure mercury intrusion techniques. *J. Nat. Gas Sci. Eng.* **2015**, *24*, 185−196.
(25) Wu, H.; Zhang, C.; Ji, Y.; Liu, R.; Cao, S.; Chen, S.; Liu, G. Pore throat characteristics of tight sandstone of Yanchang Formation in eastern Gansu, Ordos Basin. *Pet. Res.* **2018**, *3* (1), 33−43.
(26) Zou, C.; Yang, Z.; He, D.; Wei, Y.; Li, J.; Jia, A.; Chen, J.; Zhao, Q.; Li, Y.; Yang, S. Theory, technology and prospects of conventional and unconventional natural gas. *Pet. Explor. Develop* **2018**, *45* (4), 604−618.
(27) Yang, H.; Fu, J.; Liu, X. Accumulation conditions and exploration and development of tight gas in the Upper Paleozoic of the Ordos Basin. *Pet. Explor. Develop.* **2012**, *39* (3), 295−303.
(28) Zhang, C.; Li, J.; Liu, R. Microscopic characteristics and forming mechanisms of He 8th member tight sandstone gas reservoirs in the Ordos Basin. *China Pet. Explor.* **2019**, *24* (4), 476−484.
(29) Yang, H.; Xi, S.; Wei, X. Evolution and natural gas enrichment of multicycle superimposed basin in Ordos Basin. *China Pet. Explor.* **2006**, *11* (1), 17−24.
(30) Jia, L.; Zhong, D.; Sun, H. Sediment Provenance Analysis and Tectonic Implication of the Benxi Formation, Ordos Basin. *Acta Sed. Sin.* **2019**, *37* (5), 1087−1103.
(31) Washburn, E. W. The Dynamics of Capillary Flow. *Phys. Rev.* **1921**, *17* (3), 273−283.
(32) Pfeifer, P.; Avnir, D. Chemistry in nointegral dimensions between two and three. *J. Chem. Phys.* **1983**, *79* (7), 3369−3558.
(33) Mandelbrot, B. B.; Wheeler, J. A. The Fractal Geometry of Nature. *Am. J. Phys.* **1983**, *51* (3), 286−287.
(34) Dou, W.; Liu, L.; Jia, L.; Xu, Z.; Wang, M.; Du, C. Pore structure, fractal characteristics and permeability prediction of tight sandstones: A case study from Yanchang Formation, Ordos Basin, China. *Mar. Pet. Geol.* **2021**, *123*, 104737.
(35) Katz, A. J.; Thompson, A. H. Fractal sandstone pores: implications for conductivity and formation. *Phys. Rev. Lett.* **1985**, *54* (3), 1325−1328.
(36) Krohn, C. E. Sandstone fractal and euclidean pore volume distributions. *J. Geophys. Res.* **1988**, *93* (B4), 3286−3296.
(37) Qu, H.; Yang, B.; Tian, X. The primary controlling parameters of porosity, permeability, and seepage capability of tight gas reservoirs: a case study on Upper Paleozoic Formation in the eastern Ordos Basin, Northern China. *Pet. Sci.* **2019**, *16* (6), 1270−1284.
(38) Zhao, H.; Guo, Y.; Du, X.; Hu, Y.; Kang, R.; Shangguan, J. Micro-pore Multifractal Characteristics of Benxi Formation Sandstone Reservoir in Gaoqiao Area, Ordos Basin. *Bull. Geo. Sci. Tec.* **2020**, *3* (1), 33−43.
(39) Nooruddin, H. A.; Hossain, M. E.; Hasan, A.; Oksha, T. Comparison of permeability models using mercury injection capillary pressure data on carbonate rock samples. *J. Pet. Sci. Eng.* **2014**, *121*, 9−22.
(40) Xoaoth, B. B. Coal and gas outburst. In: Song, S.; Wang, Y., Translation, Beijing, *China Ind. Pre.* 1966.
(41) Susan, K. C.; Amnon, B. I.; John, G.; Lynsey, P.; Jaegun, J.; Wilson, S.; Jim, M.; Greg, Y. Ozone Impacts of Natural Gas Development in the Haynesville Shale. *Environ. Sci. Tec.* **2010**, *44* (24), 9357−9363.
(42) Pittman, E. D. Relationship of porosity and permeability to various parameters derived from mercury injection capillary pressure curves for sandstone. *AAPG Bull.* **1992**, *76*, 191−198.
(43) Nabawy, B. S.; Geraud, Y.; Rochette, P.; Bur, N. Pore-throat characterisation in highly porous and permeable sandstones. *AAPG Bull.* **2009**, *93* (6), 719−739.
(44) Mahamud, M. M.; Novo, M. The use of fractal analysis in the textural characterisation of coals. *Fuel* **2008**, *87* (2), 222−231.
(45) Yin, X.; Jiang, S.; Chen, S.; Wu, P.; Gao, W.; Gao, J.; Shi, X. Impact of rock type on the pore structures and physical properties within a tight sandstone reservoir in the Ordos Basin, NW China. *Pet. Sci.* **2020**, No. 1, 33−43.
(46) Peng, S.; Zhang, T.; Loucks, R. G.; Shultz, J. Application of mercury injection capillary pressure to mudrocks: conformance and compression corrections. *Mar. Pet. Geol.* **2017**, *88*, 30−40.

https://dx.doi.org/10.1021/acs.energyfuels.0c03991
Energy Fuels 2021, 35, 3887−3898